Measured High-Resolution Power-Delay Profiles of Nonstationary Vehicular Millimeter Wave Channels

Jiri Blumenstein*, Ales Prokes*, Josef Vychodil*, Tomas Mikulasek*, Jiri Milos*,
Erich Zöchmann†‡, Herbert Groll‡, Christoph F. Mecklenbräuker‡,
Markus Hofer^x, David Löschenbrand^x, Laura Bernadó^x,
Thomas Zemen^x, Seun Sangodoyin††, Andreas Molisch††

* Department of Radio Electronics, Brno University of Technology, Czech Republic, *blumenstein@vutbr.cz*
† Christian Doppler Laboratory for Dependable Wireless Connectivity for the Society in Motion
‡ Institute of Telecommunications, TU Wien, Austria
^x Safety and Security Department, Austrian Institute of Technology, Austria
†† Wireless Devices and Systems Group, University of Southern California, USA

***Abstract*—This paper reports on a power-delay profile measurement campaign emulating a mobile vehicle-to-infrastructure urban-highway environment. The measured location is in the city of Brno, Czech Republic. Utilizing a correlative 50 GS/s time-domain channel sounder with a center frequency of 59.6 GHz and 8 GHz bandwidth and with open-ended WR15 waveguide antennas, we characterize the representative millimeter wave radio channels in terms of the RMS delay spread and its variability caused by mobile scatterers (i.e., vehicles). The RMS delay spread exhibits notable heteroscedasticity as its standard deviation can decrease by 40%. The measured high resolution power-delay profiles exhibit clustering behavior, where a typical number of reflected multipath components is four to five.**

I. Introduction

Considering vehicle-to-infrastructure (V2I) communications, the license-free millimeter-wave (mmwave) band with 60 GHz center frequency offers several GHz of bandwidth, which is unrivaled to the traditional V2I bands (around 760 MHz or 5.9 GHz [1]). In addition, due to advances in mmwave sampling hardware, broadband vehicular mmwave communications has recently re-gained significant attention [2]. The research of mmwave radio propagation intended for vehicular communication has been going on for several decades; however, mostly as narrowband systems. Meinel and Plattner [3] were analyzing a narrowband mmwave communication system for a infrastructure to train scenario already in 1983. Akihito et al. [4] were investigating (also narrowband) 60 GHz car-to-car communications in 2001. In [5], [6] path-loss results demonstrate a two-ray fading behavior. Additional effects of road surfaces have been investigated in [7]–[9].

Broadband vehicle-to-vehicle measurements (with 500 MHz bandwidth) are described in [10], where measured delay and Doppler profiles of overtaking vehicles in the 60 GHz band are presented; however, the time-varying power-delay profile behavior is not discussed and the antenna placement does not match the intended V2I scenario. In [11], delay and Doppler spreads of non-stationary vehicular 4×4 multiple-input multiple-output (MIMO) channels are researched; however, the frequency band is 5480-5520 MHz. The effect of vibrations caused by the road surface quality or by the engine operation is evaluated via delay-Doppler spreading functions with several GHz of bandwidth in [12].

The analysis of static mmwave channels is already well researched, see e.g. [13]–[15], where a K-factor and root mean square (RMS) delay spread are evaluated for indoor channel. In [16], a MIMO intra-vehicular channel with a 10 GHz bandwidth is studied. Contrarily, channel sounding concepts for dynamic scenarios have only recently been proposed [17], [18]. With this background, the contributions of this paper are following:

- We provide exemplary power-delay profiles for a typical V2I scenario considering a vehicular broadband mmwave channel.
- Moreover, we provide analysis of the RMS delay spread, which is affected by the passing vehicles and thus exhibiting heteroscedasticity, i.e. a notable RMS delay spread standard

deviation variations over the measured time period.

- We also present a time-domain channel sounder, which consists from off-the-shelf parts and laboratory devices such as an oscilloscope or a bit sequence generator.

II. Scenario Description

The measured V2I site is located in the city of Brno, Czech Republic. The campaign was conducted in a urban-highway environment, where we have emulated the mmwave communication with an overhead (roadside) infrastructure. Obviously, the higher the infrastructure access point is mounted, the higher is the possibility to experience a line-of-sight propagation towards the passing vehicles. In our case, the TX is placed at our emulated toll-gate, where its height above the road is around 5 m. The RX is placed at the ground level with the antenna height of 1.6 m. The photographs of the scene are depicted in Figure 2a.

Both the RX and TX are static; however, the traffic passing through the measured scene, effectively creating a moving scatterers, could represent an overtaking maneuver of a vehicle imitated by the RX. We assume that reflections with the receiver car are below the receiver noise floor. Therefore, the receiver car is omitted and replaced by a simpler tripod mounting. The blue car (in Figure 2a only the rear part is visible) serves as a carrier of the RX hardware and is not part of the measured scenario.

III. Channel sounder

In this section we provide a description of the in-house built (from off-the-shelf components and laboratory devices) channel sounder including a basic theoretical background of the time-domain channel sounding. A similar setup has been utilized in our contributions [9], [12], [19]; however, the channel sounder utilized in this paper is different as it consists from separate TX and RX sides. The 10 MHz synchronization is done via a coaxial cable.

A. Principle of the channel sounder operations

The correlative channel sounder captures the transmission channel in the time domain. Another possibility is to perform the channel sounding in the frequency domain, where the sounder usually requires notable amount of time to sweep the measured band [20]. On the other hand, the time domain channel sounding usually transmits a broadband pulse or sequence and the need for the channel sweep time is mitigated. As a result, the time domain sounding is much more suitable for time-variant channels, which is the case of the measured V2I scenario.

The time-variant channel is characterized by the channel impulse response (CIR) and is written as [21]:

$$h(t,\tau) = \sum_{n=1}^{N(t)} \alpha_n(t) e^{j2\pi f t} \delta\left(\tau - \tau_n(t)\right), \qquad (1)$$

where N is the number of propagation paths. Note that in this measurement campaign, due to the antenna installation, the line-of-sight (LOS) components $h_{\mathrm{LOS}}(t,\tau)$ are always present. The summation with the multipath components (MPCs) $h_{\mathrm{MPC}}(t,\tau)$, i.e.:

$$h(t,\tau) = h_{\mathrm{LOS}}(t,\tau) + h_{\mathrm{MPC}}(t,\tau), \qquad (2)$$

creates an alternative formula to (1). Correlative channel sounders often exploit properties of pseudo-noise sequences. In this paper, we employ Golay sequences [22] with autocorrelation R_{xx} forming a distinct triangular function. For the purpose of our measurement; however, we simplify to $R_{xx} \approx \delta(\tau)$. Thus, it is possible to write:

$$y(t) = h(t) \otimes x(t), \qquad (3)$$

where $y(t)$ is the received signal, $x(t)$ represents the transmitted Goaly sequence and finally $\otimes$ denotes the linear convolution.

Since the transmitted Golay sequence is known to the RX, it is possible to estimate the CIR from the cross-correlation of the transmitted and received signals $x(t)$ and $y(t)$ due to:

$$R_{xy}(\tau) = \mathrm{E}\{x^*(t)y(t)\} = h(t) \otimes R_{xx}(\tau) \approx \\ \approx h(t) \otimes \delta(\tau) = h(t), \qquad (4)$$

where $\mathrm{E}\{\}$ denotes for the expected value operator.

B. Measurement devices

The block scheme of the time-domain channel sounder is depicted in Figure 1. Note that the channel sounder is composed from off-the-shelf parts and laboratory devices. As a sampling device, we use a oscilloscope Tektronix MSO72004C performing as a matched receiver with 50 GS/s sampling frequency and 16 GHz bandwidth. This signal is filtered in the baseband with a microstrip low-pass filter with 8 GHz bandwidth.

As for the TX, the Anritsu Signal Quality Analyzer MP1800A generates Golay sequences with 13 dBm output power and data rate 12.5 Gbit/s. To improve the dynamic range, the low-noise and power amplifiers QuinStar QLW-50754530-I2 and QPW-50662330 were used. We also utilized the Sivers IMA FC1003V/01 up and down converter to move the signal to the band of interest.

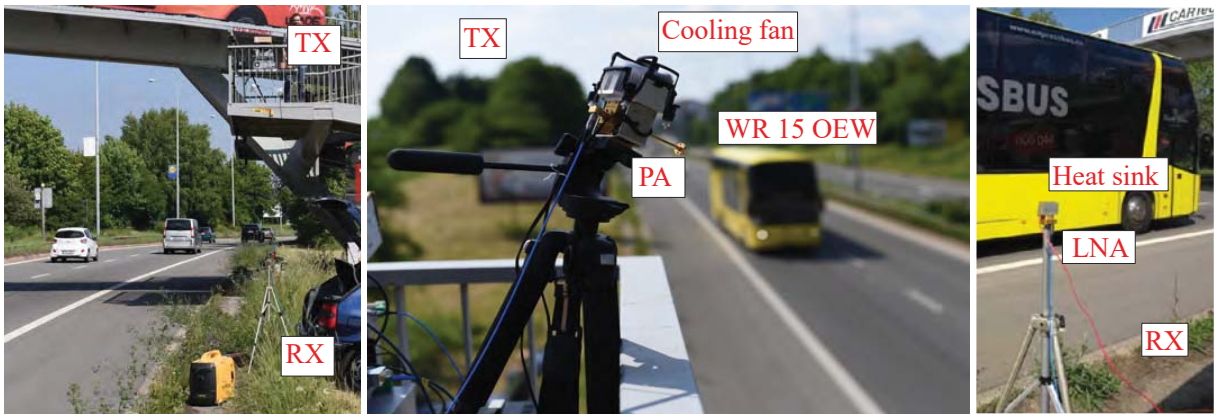

Fig. 1: Photographs of the measurement site. TX side is elevated 5 m above the four-lane highway (counting both directions, equipped with a metallic central barrier), emulating overhead roadside infrastructure installation, while RX is located on the side of the road (antenna height is 1.6 m). The vehicles driving by the RX apparatus emulate the overtaking maneuver.

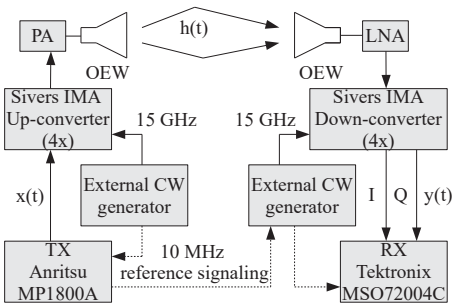

(a) Time-domain correlative channel sounder utilizing Golay sequences, stable external RF source and a matched receiver.

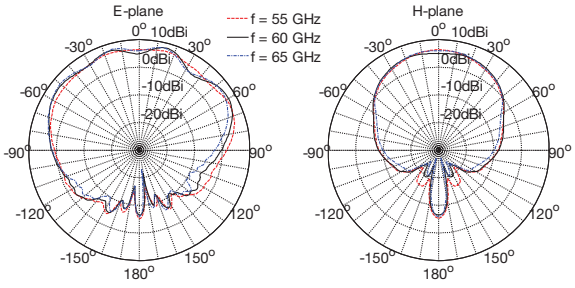

(b) Measured gain pattern of the open-ended WR15 waveguide in the E–plane and the H–plane for the 55-65 GHz frequency range.

Fig. 2: Channel sounder and utilized WR 15 OEW antennas.

C. Real-time data processing

The transmitted Golay sequence consists of two complementary sequences a and b. In our case, the length of both sequences is $\mathrm{L} = 2048$. Now, the Golay pair is transmitted twice (forming a cyclic prefix-like pattern), meaning that the total length of the pair is $4\mathrm{L}$. The utilization of Golay pairs leads to reduced side-lobes in the correlation domain. Moreover, a method utilizing a second Golay pair with inverted polarity is used in order to further mitigate even-order spurious interferences. The transmitted signal obeys the following pattern: $[a, a, b, b, -a, -a, -b, -b]$. Hence, the total length of the transmitted sequence is $8\mathrm{L}$ symbols. This signal is then up-sampled with a factor of four, leading to $4 \times 8\mathrm{L} = 65536$ samples. More information about this method and the channel sounder is in [23].

Taking into account that we employ 50 GS/s sampling frequency and that the internal memory of the oscilloscope is 31.25 MS, we are able to capture 492 channel snapshots into the fast internal memory of the oscilloscope. The 492 channel snapshots form a power-delay profile (PDP) recording. Between each channel recording, there is a pause required for data download.

IV. Measurement Result

The measurement results are represented by a set of time-varying PDP recordings, where each recoding captures approx. 0.5 s with a sampling frequency of $1/820\ \mu$s in the time domain (in the delay domain, the sampling is $1/20$ ps). Due to a relatively short duration of the recording, we took a photograph of the scene both from the RX and TX positions. Thus, we obtain information about the vehicle's configuration on the road and their individual type and size.

A. U-shaped reflections

The exemplary PDPs are depicted in Figure 3. In Figure 3a, the LOS component is visible together with the reflection from a metallic central barrier, effectively forming a clutter (as known from the radar signal processing). The moving vehicles are distinctly

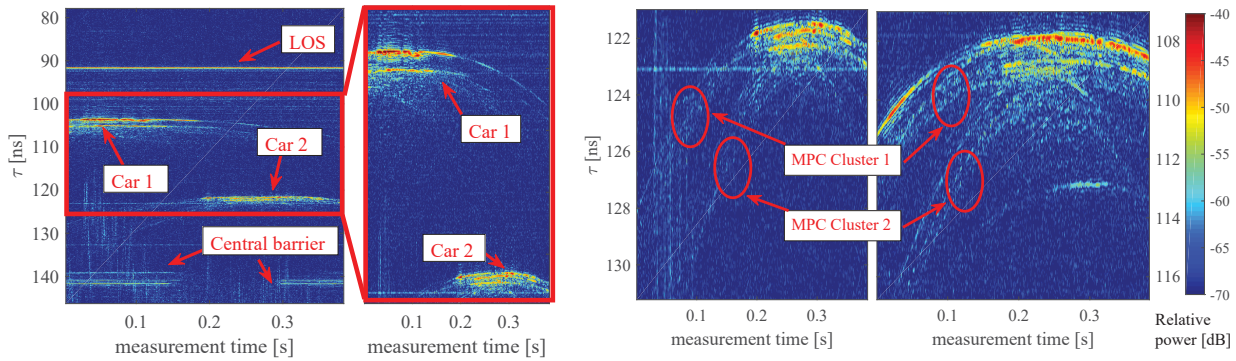

(a) The moving vehicles induce a shadowing effect. Therefore, between $t = 0.15\,\mathrm{s}$ and $t = 0.30\,\mathrm{s}$, the reflection from the central barrier vanishes, consequently the RMS delay spread exhibits heteroscedasticity.

(b) Multiple reflections originating from a single vehicle and forming a clusters 1 and 2 of the multipath components with similar delay domain characteristics.

Fig. 3: Representative example of time-varying power-delay profiles.

visible as the U-shaped MPC clusters. The U-shape is determined by the vehicle speed and its radar cross-section. In the majority of cases, the dead center (where the MPC delay is minimized) of the U-shaped MPC cluster is the most powerful part of the vehicle's reflection. The dead center of the U-shaped MPCs cluster exhibits the smallest accumulated distance (TX-reflection-RX) among other reflections originating from a single vehicle. Therefore, we deduce that the strongest reflections come from the side of the passing vehicle, as this configurations forms a isosceles triangle (from TX to the reflection and finally to the RX). This implies that the simplistic geometrical optics and the Snell's law is to a certain extend relevant also in the mmwave propagation description. In the case of long vehicles, e.g. buses, the middle part of the U-shaped reflections are straightened and forms a line in the PDP.

B. Heteroscedasticity of the RMS delay spread

The sudden presence of a strong reflector or even a number of strong reflectors has its implications to the normalized second-order central moment of the PDP, i.e. to the RMS delay spread. In Figure 4, we compare 8 superimposed PDP recordings, where the mean RMS delay spread is around 3.5 ns and was determined considering a static measured scene, i.e. without vehicles. Note, that here we do not consider e.g. the effects of wind and other minor sources of variability. The presence of a strong reflecting object can alter the RMS delay spread notably. In our case, the presence of vehicles reduce the RMS delay spread from the 3.5 ns by 1.5 ns, meaning that the reduction is around 40%. Thus, the RMS delay spread exhibits heteroscedasticity. The presence of cars induce the strong MPC clusters at short delays, the energy is hence more concentrated close to the LOS delay.

C. Shadowing and MPC Clustering

In Figure 3a, we can see a shadowing effect, where the presence of car 1 and car 2 causes the central barrier reflection to disappear. In Figure 3b, several reflections originating from a single vehicle are visible. Moreover, some reflections are parallel, showing similar delay-domain characteristics and thus forming a MPC cluster. Typical number of distinct reflections from a single vehicle are 4 to 5 reflections.

V. Conclusion

We have conducted first broadband (with 8 GHz bandwidth) V2I mmwave channel measurements demonstrating the power-delay profiles of the vehicles passing through the measurement scene. We have considered a V2I scenario with an overhead access point installation. The measured data shows notable heteroscedasticity of the RMS delay spread caused by a stochastic appearance of strongly reflecting objects (cars passing through the measurement location). Moreover, we show that a passenger car usually reflects a number of MPCs with similar characteristics, thus showing distinct clustering behavior.

Acknowledgment

The research described in this abstract was financed by the Czech Science Foundation, Project No. 17-27068S, and by the National Sustainability Program under grant LO1401. For the research, the infrastructure of the SIX Center was used. The financial support by the Austrian Federal Ministry of Science, Research and Economy and the National Foundation

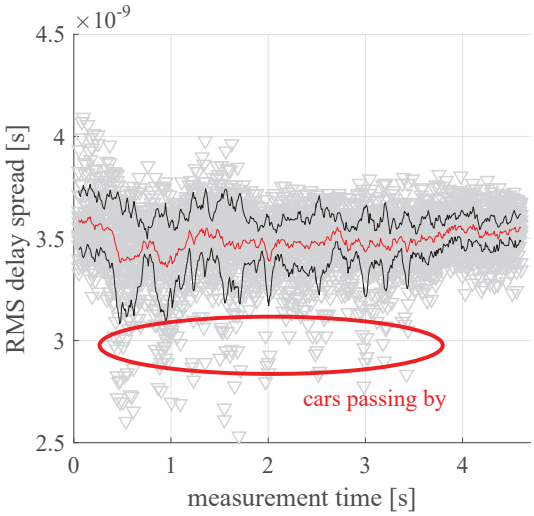

Fig. 4: The measured RMS delay spread variations of 8 superimposed PDP recordings, each capturing one or two cars in the measured scene. The mean value of the RMS delay spread is depicted as the red curve with ± of its standard deviation (black curves). Vehicles passing by the emulated communication link cause a RMS delay spread heteroscedasticity.

for Research, Technology and Development is gratefully acknowledged. The work of S. Sangodoin and A. F. Molisch was supported by the NSF and NIST. This work was carried out in the framework of COST Action CA15104 IRACON.

REFERENCES

[1] J. Harding, G. Powell, R. Yoon, *et al.*, "Vehicle-to-vehicle communications: Readiness of V2V technology for application," Tech. Rep., 2014.

[2] V. Va, T. Shimizu, G. Bansal, *et al.*, "Millimeter wave vehicular communications: A survey," *Foundations and Trends in Networking*, vol. 10, no. 1, pp. 1–113, 2016.

[3] H. Meinel and A. Plattner, "Millimetre-wave propagation along railway lines," *IEE Proceedings F (Communications, Radar and Signal Processing)*, vol. 130, no. 7, pp. 688–694, 1983.

[4] K. Akihito, S. Katsuyoshi, M. Fujise, *et al.*, "Propagation characteristics of 60-GHz millimeter waves for ITS inter-vehicle communications," *IEICE Transactions on Communications*, vol. 84, no. 9, pp. 2530–2539, 2001.

[5] S. Takahashi, A. Kato, K. Sato, *et al.*, "Distance dependence of path loss for millimeter wave inter-vehicle communications," *Radioengineering*, vol. 13, no. 4, p. 9, 2004.

[6] A. Yamamoto, K. Ogawa, T. Horimatsu, *et al.*, "Path-loss prediction models for intervehicle communication at 60 GHz," *IEEE Transactions on Vehicular Technology*, vol. 57, no. 1, pp. 65–78, 2008.

[7] K. Sarabandi, E. S. Li, and A. Nashashibi, "Modeling and measurements of scattering from road surfaces at millimeter-wave frequencies," *IEEE Transactions on Antennas and Propagation*, vol. 45, no. 11, pp. 1679–1688, 1997.

[8] A. Yamamoto, K. Ogawa, T. Horimatsu, *et al.*, "Effect of road undulation on the propagation characteristics of inter-vehicle communications in the 60 GHz band," in *Proc. of IEEE/ACES International Conference on Wireless Communications and Applied Computational Electromagnetics*, 2005, pp. 841–844.

[9] J. Blumenstein, A. Prokes, J. Vychodil, *et al.*, "Time-varying K factor of the mm-Wave vehicular channel: Velocity, vibrations and the road quality influence," in *2017 IEEE 28th Annual International Symposium on Personal, Indoor, and Mobile Radio Communications (PIMRC)*, Oct. 2017, pp. 1–5.

[10] E. Zöchmann, C. F. Mecklenbräuker, M. Lerch, *et al.*, "Measured delay and Doppler profiles of overtaking vehicles at 60 GHz," in *Proc. of the 12th European Conference on Antennas and Propagation (EuCAP)*, pp. 1–5.

[11] L. Bernadò, T. Zemen, F. Tufvesson, *et al.*, "Delay and Doppler spreads of nonstationary vehicular channels for safety-relevant scenarios," *IEEE Transactions on Vehicular Technology*, vol. 63, no. 1, pp. 82–93, Jan. 2014.

[12] A. Prokes, J. Vychodil, M. Pospisil, *et al.*, "Time-domain nonstationary intra-car channel measurement in 60 GHz band," in *2016 International Conference on Advanced Technologies for Communications (ATC)*, Oct. 2016, pp. 1–6.

[13] E. Zöchmann, M. Lerch, S. Caban, *et al.*, "Directional evaluation of receive power, Rician K-factor and RMS delay spread obtained from power measurements of 60 GHz indoor channels," in *Proc. of IEEE-APS Topical Conference on Antennas and Propagation in Wireless Communications (APWC)*, 2016.

[14] J. Vehmas, J. Jarvelainen, S. L. H. Nguyen, *et al.*, "Millimeter-wave channel characterization at Helsinki airport in the 15, 28, and 60 GHz bands," in *Proc. of IEEE Vehicular Technology Conference (VTC-Fall)*, 2016.

[15] F. Fuschini, S. Häfner, M. Zoli, *et al.*, "Analysis of in-room mm-Wave propagation: Directional channel measurements and ray tracing simulations," *Journal of Infrared, Millimeter, and Terahertz Waves*, vol. 38, no. 6, pp. 727–744, 2017.

[16] J. Blumenstein, A. Prokes, A. Chandra, *et al.*, "In-vehicle channel measurement, characterization, and spatial consistency comparison of 30–11 GHz and 55–65 GHz frequency bands," *IEEE Transactions on Vehicular Technology*, vol. 66, no. 5, pp. 3526–3537, May 2017.

[17] P. B. Papazian, C. Gentile, K. A. Remley, *et al.*, "A radio channel sounder for mobile millimeter-wave communications: System implementation and measurement assessment," *IEEE Transactions on Microwave Theory and Techniques*, vol. 64, no. 9, pp. 2924–2932, 2016.

[18] E. Zöchmann, S. Caban, M. Lerch, *et al.*, "Resolving the angular profile of 60 GHz wireless channels by delay-Doppler measurements," in *Proc. of IEEE Sensor Array and Multichannel Signal Processing Workshop (SAM)*, 2016, pp. 1–5.

[19] J. Blumenstein, J. Vychodil, M. Pospisil, *et al.*, "Effects of vehicle vibrations on mm-wave channel: Doppler spread and correlative channel sounding," in *2016 IEEE 27th Annual International Symposium on Personal, Indoor, and Mobile Radio Communications (PIMRC)*, Sep. 2016.

[20] A. Chandra, A. Prokes, T. Mikulášek, *et al.*, "Frequency-domain in-vehicle UWB channel modeling," *IEEE Transactions on Vehicular Technology*, vol. 65, no. 6, pp. 3929–3940, Jun. 2016.

[21] F. Hlawatsch and G. Matz, *Wireless communications over rapidly time-varying channels*. Academic Press, 2011.

[22] M. Golay, "Complementary series," *IRE Transactions on Information Theory*, vol. 7, no. 2, pp. 82–87, Apr. 1961.

[23] J. Vychodil, M. Pospisil, A. Prokes, *et al.*, "Millimeter wave band time domain channel sounder," *IET Communications-submitted*, 2018.